

Arthrographic description of the canine carpal joint cavities and its recesses

Sven Klußmann^{1,2}  | Andrea Meyer-Lindenberg¹  | Andreas Brühschwein¹ 

¹Clinic for Small Animal Surgery and Reproduction, LMU Munich, Munich, Germany

²Equine Clinic, LMU Munich, Munich, Germany

Correspondence

Sven Klußmann, Equine Clinic, LMU Munich, Munich 85764, Germany.
Email: sven.klussmann@lmu.de

Abstract

Joint effusion is diagnostically important. The canine carpal joint effusion, which is sometimes difficult to detect clinically, has received less attention in diagnostic ultrasound (US) studies. The aim of the present study was to provide a description of the morphological appearance of the canine carpal joint cavities and recesses using US, radiography, helical computed tomography (CT) and three-dimensional volume rendering technique (3D-VRT) images and to prove the applicability of musculoskeletal US for the detection of artificial carpal joint effusion in dogs. The understanding of the characteristics of these structures in normal patients is essential in the diagnosis. Twenty-eight clinically and radiologically unremarkable canine carpal cadavers of different breeds were examined, representative images were selected and anatomical structures were labelled. The canine carpal joint cavities and in particular its recesses had a complex appearance with a basic structure found in all dogs: Antebrachiocarpal joint: dorsoproximal antebrachiocarpal recess, dorsodistal antebrachiocarpal recess, medial antebrachiocarpal recess, lateral antebrachiocarpal recess and five palmar antebrachiocarpal recesses. Middle carpal joint: two dorsal middle carpal recesses, medial common middle carpal and carpometacarpal recess, lateral common middle carpal and carpometacarpal recess, four palmar middle carpal recesses. The carpometacarpal joint had dorsal and palmar funnel-shaped and irregular, finely tubular extensions, the most prominent ran dorsal to metacarpal III, the maximum distal end represented the proximal metacarpal diaphysis. All recesses presented ultrasonographically as a generalized anechogenic to hypoechoic filled continuation of the articular capsule with an indistinct peripheral hypoechoic to isoechogenic fine capsule, the synovial-connective tissue interface was difficult to identify. The novel results of this study provide the first morphological description of the ultrasonographic, radiographic and computed tomographic arthrographic appearance of the canine carpal joint cavities and recesses with different injection volumes. The canine carpal joint cavities and in particular its recesses had a complex appearance with a basic structure found in all dogs. The applicability of musculoskeletal US to visualize an artificial carpal effusion has been demonstrated. The results of this study, and in particular US, give the

This is an open access article under the terms of the [Creative Commons Attribution](https://creativecommons.org/licenses/by/4.0/) License, which permits use, distribution and reproduction in any medium, provided the original work is properly cited.

© 2024 The Authors. *Anatomia, Histologia, Embryologia* published by Wiley-VCH GmbH.

practitioner an advantage in visualizing joint effusion and assist in the decision to perform arthrocentesis.

KEYWORDS

arthrography, canine, carpus, computed tomography, joint capsule, ultrasound

1 | INTRODUCTION

The canine carpus with its seven carpal bones, arranged in two rows and held together by a multitude of carpal ligaments, is a complex joint and functions as a ginglymus (Yalden, 1970). These structures can be damaged by many causes and lead to forelimb lameness (Marcellin-Little & von Pfeil, 2020).

Traumatic hyperextension is a common injury and often results in multiligamentous pathology (Bristow et al., 2015), the radiocarpal and the carpometacarpal joints are most commonly involved (Denny & Barr, 1991; Parker et al., 1981). Fractures (DeCamp et al., 2016; Johnson, 1987; Li et al., 2000) and soft tissue diseases like carpal sprain injuries (Guilliard, 1997; Guilliard & Mayo, 2000) are described. Rare diseases are the neurofibroma of the ulnar nerve in the carpal canal (Basa et al., 2020) or the solitary osseous plasmacytoma of the second and third carpal bones (Reising et al., 2021). Interest in canine carpus research is diverse (Adams et al., 2005). Experimental cadaveric studies of the carpal hyperextension complex are described with regard to the kinematics of the antebrachiocarpal joint, the palmar radiocarpal ligament and the palmar ulnocarpal ligament (Milgram et al., 2019; Neville-Towle et al., 2018). Several surgical treatment options have been investigated, including partial carpal arthrodesis and panarthrodesis (Haburjak et al., 2003; Jerram et al., 2009; Parker et al., 1981; Théoret & Moens, 2007; Willer et al., 1990). The diagnostic workup of canine carpal lameness is classically based on orthopaedic and radiographic examinations, including stress radiography techniques as well as arthrocentesis and are sufficient in most cases to achieve an accurate diagnosis (Farrow, 1982; Marcellin-Little & von Pfeil, 2020; Tobolska et al., 2020). Injuries or mild loss of mineralized bone may be difficult or impossible to detect radiographically, direct visualization of soft tissue opaque structures such as cartilage or synovial fluid cannot be obtained in radiography with only periarticular and subchondral changes discernible (Allan & Davies, 2018). Arthroscopy of the antebrachiocarpal joint is described as a useful adjunct to standard diagnostic modalities (Warnock & Beale, 2004). US is described for the anatomy of the dorsal (González-Rellán et al., 2021) and palmar region (González-Rellán et al., 2023) or in the case of stenosing tenosynovitis of the abductor pollicis longus muscle (Hittmair et al., 2012). Advanced imaging such as magnetic resonance imaging (MRI) is used for carpal ligaments visualization (Castelli et al., 2019; Nordberg & Johnson, 1999) or for the diagnosis of the avascular necrosis of the intermedioradial carpal bone (Pownder et al., 2016). CT arthrography improves soft tissue differentiation and has successfully used for enhancing the appearance of the feline carpal ligaments (Basa et al., 2022) or as useful adjunct to surgery CT to find a diagnosis in the canine shoulder (Eivers et al., 2018).

Joint diseases are often associated with increased joint fluid in response to injury or inflammation (Rondeau et al., 2005; Vaughan, 1985). Immune mediated arthritis and its subtypes are a common form of carpal arthritis (Shaughnessy et al., 2016). Joint effusion with arthrocentesis and synovial fluid examination plays a key role in further differentiation and classification of joint disease (Harris & Santangelo, 2020). However, joint effusion can be difficult or even impossible for the examiner to detect clinically (Rondeau et al., 2005), which may influence the decision to use arthrocentesis in everyday clinical practice. The physiological carpal synovial volume is described as a drop of up to 1 mL (Clements, 2006; Cowell & Valenciano, 2014; Whitelock, 2001), canine carpal joint fluid or effusion has received less attention in diagnostic ultrasound studies. In horses, joint effusion can be reliably diagnosed by ultrasonography (Beccati et al., 2015). Morphological and imaging studies of the carpal joint cavity in horses (Ford et al., 1988; Gerdes et al., 2022; Getman et al., 2007; Gray et al., 2013; McQuillan et al., 2022; Suarez Sanchez-Andrade et al., 2018; Tnibar et al., 1993) and donkeys (Alsafy et al., 2015; El-Gendy et al., 2020) are described in various ways. In dogs, there is no imaging study with description of the carpal joint cavity and its recesses in healthy dogs, ultrasonographic studies on carpal joint effusion are lacking. Therefore, the aim of the present study was (1) to provide a description of the morphological appearance of the canine carpal joint cavities and recesses using US, radiography, helical CT and 3D-VRT arthrography images, (2) to prove the applicability of musculoskeletal US for the detection of carpal joint effusion in dogs.

2 | MATERIALS AND METHODS

The study design was prospective and descriptive. A structured flow chart with a detailed description of materials and methods is shown in Figure 1. All dogs used in this study were dead due to other reasons unrelated to this study, the owners have provided the dogs for teaching and research purposes. The study was conducted in accordance with the local legislation, all procedures were performed in accordance to animal care committee requirements.

2.1 | Canine carpal cadavers

A total of 38 canine carpal cadavers from 19 dogs of different breeds were collected. Carpal cadaver processing procedure: after an unremarkable orthopaedic and radiographic examination

in two planes, the forelimb was dissected proximal to the elbow, tightly placed adhesive tape prevented air entrapment and slippage of soft tissue structures distally (Figure 2). Due to continuous hospital operations and available refrigeration and storage facilities, freshly collected limbs were stored frozen (-12°C) for a maximum of 2 weeks. The hair was carefully clipped from the entire carpus and the skin was washed with soap. After thawing to room temperature, each carpus was radiographed again in two planes and examined by US and CT to rule out musculoskeletal disorders, particularly soft tissue damage or air entrapment during freezing and storage.

2.2 | Arthrocentesis and arthrography

Arthrocentesis and arthrography were carried out on the antebrachiocarpal joint and the middle carpal joint, but not on the carpometacarpal joint. A puncture of the carpometacarpal joint was not performed due to the described connection between the

middle carpal joint and the carpometacarpal joint (König et al., 2007; Salomon, 2020).

Arthrocentesis was performed flexed using anatomical landmarks (Vollmerhaus, 2007) under fluoroscopic guidance. The puncture of the antebrachiocarpal joint was performed 3–5 mm distal to the trochlea of radius at the lateral edge of the tendon of the extensor carpi radialis muscle and medial to the accessory cephalic vein. The needle was inserted vertically through the skin and advanced obliquely in a mediopalmar direction. The puncture of the middle carpal joint was performed 2–4 mm distal to the joint edge of the intermedioradia carpal bone, at the lateral edge of the tendon of the extensor carpi radialis muscle and medial to the accessory cephalic vein. The needle was considered to be safely intra-articular if the bevel of the needle was in the respective centre of the joint space. Aspiration of synovial fluid before the first contrast agent (CA) injection was performed and recorded.

For arthrography, the non-ionic, monomeric, triiodinated, water-soluble CA iohexol (Accupaque 300, GE Healthcare

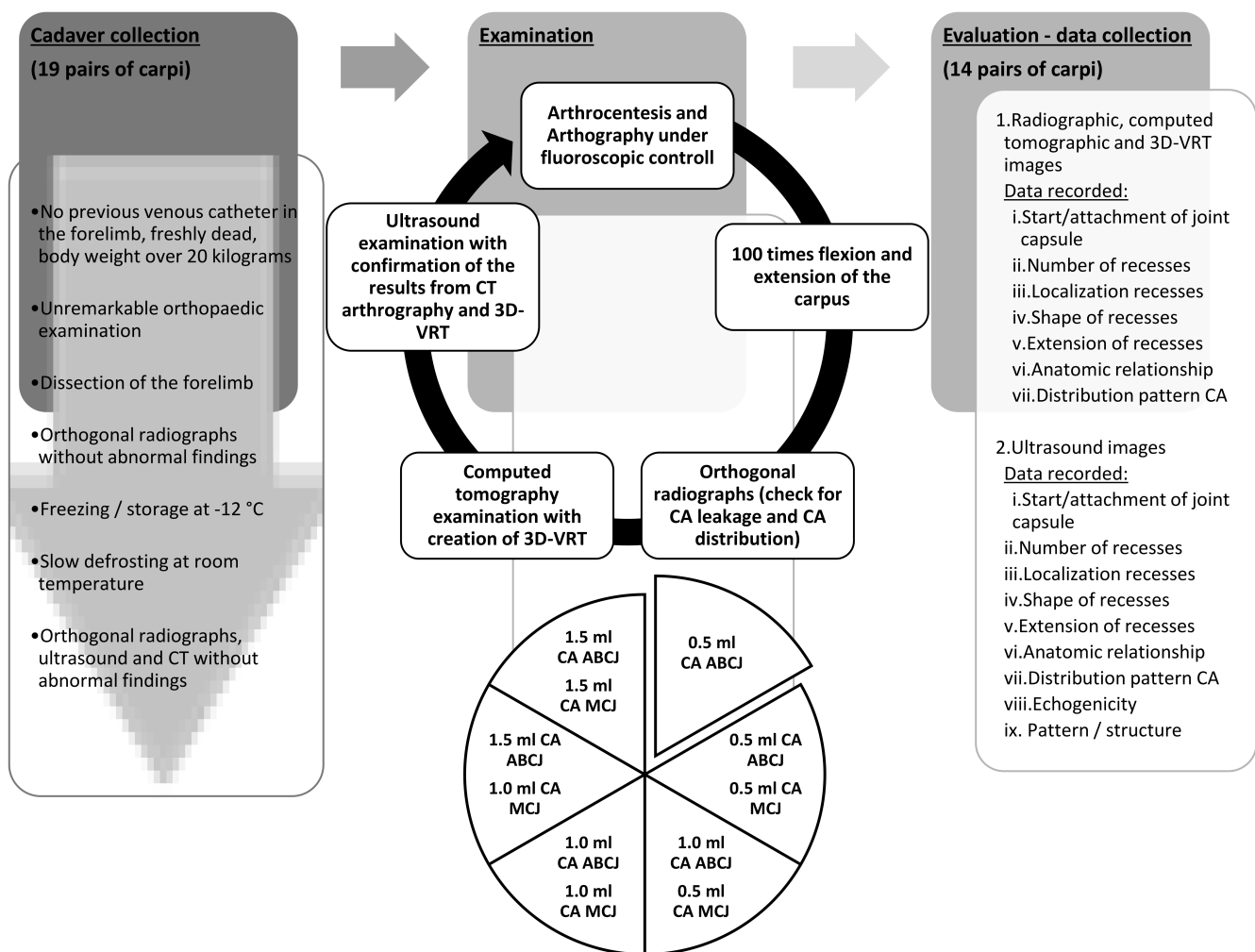


FIGURE 1 Flowchart materials and methods. ABCJ: antebrachiocarpal joint; CA, Contrast agent; MCJ, middle carpal joint; 3D-VRT: Three-dimensional volume rendering technique.



FIGURE 2 Cadaver preparation. The forelimb was dissected proximal to the elbow (a), tightly placed adhesive tape prevented air entrapment and slippage of soft tissue structures distally (b).

Buchler GmbH & Co. KG, Braunschweig, Germany) was diluted by 50% with saline solution for an iohexol concentration of 323,5 mg/mL, which corresponds to a bound iodine concentration of 150 mg iodine/mL. CA concentration was based on veterinary and human reference values to avoid beam hardening (Castelli et al., 2019; De Rycke et al., 2015; Moser et al., 2007; Samii et al., 2009). The diluted CA was warmed up by hand to body temperature for better viscosity. Under fluoroscopic control, 0.5 mL of diluted CA was injected three times into the antebrachiocarpal and middle carpal joint using a 27 g needle, six graded joint fillings were created. After each injection, the carpus was flexed and extended for 100 times to ensure adequate CA distribution, radiographic control for extraarticular contrast leakage and contrast distribution in a dorsopalmar and mediolateral view was performed and CT and US images were acquired. Joints with extravasation more than the needle tract with a small drop-shaped extraarticular

leak were excluded. Contrast injection was discontinued as soon palpable resistance was sensed during pressure on the syringe plunger or contrast backflow was identified on fluoroscopy. Twenty-eight canine carpal cadavers from 14 dogs (7 bitches and 7 dogs; age in years: 1–12, $\bar{\sigma}$ 8,05; size in kg: 22–40, $\bar{\sigma}$ 30,1) met all the inclusion criteria for examination and data collection: no previous venous catheter in the forelimb, freshly dead, body weight over 20 kg, carpi were present in pairs, orthopaedic, ultrasonographic, radiographic and computertomographic examination without evidence of musculoskeletal respectively soft tissue disorders in the carpal region or severe extravasation. All dogs were companion animals, neutered, and the breeds included three crossbreeds, two German Boxers, two Golden Retrievers, a Labrador Retriever, a Hungarian Short-Haired Pointer, a Siberian Husky, an Entlebucher Mountain Dog, a German Shepherd, a Border Collie and a Doberman Pinscher.

2.3 | CT examination

All examinations were performed with the 64-slice helical CT scanner SOMATOM Definition AS, CT070/13/S, from Siemens AG (Siemens Healthcare GmbH, Erlangen, Germany) with parameters of 140 mAs, 120 kV, 512 × 512 image size matrix, 0.6 mm reconstructed slice thickness, 0.6 mm reconstruction intervall, rotation time 0.5 s, field of view as small as possible, but as large as necessary and kernel settings of B30s and B70s for all acquired data. Each carpus was positioned in head-first prone position on the CT table. The region of interest was set using a topogram and included the region from the distal third of the antebrachium to the middle third of the metacarpus. The canine carpus DICOM (Digital Imaging and Communications in Medicine) studies were multiplanar reconstructed in transverse, sagittal, and dorsal planes at syngo CT Workplace (Siemens Healthcare GmbH, Erlangen, Germany), the colour image creation of the 3D-VRT (standard presetting: osseus transparent metal, Siemens Healthcare GmbH, Erlangen, Germany) was used for visualization of the joint capsules and recesses. The following data were collected: start/attachment of joint capsule, number of recesses, localization of recesses, shape of recesses, extension of recesses, anatomic relationship and distribution pattern of CA.

2.4 | US examination

The carpus was systematically divided into four surfaces in dorsal, palmar, medial, and lateral and examined ultrasonographically in transverse, sagittal and oblique planes from the distal third of the antebrachium to the proximal third of the metacarpus by a wide-band interoperative linear array transducer (L8-L18i-D Hockey Stick Probe, GE Healthcare, Solingen, Germany) without a standoff pad at an US



FIGURE 3 Radiographic and fluoroscopic (inverted) images of the arthrogram. 0.5 mL CA was injected with a 27 G needle in the dorsal and flexed approach into the antebrachiocarpal (a) and middle carpal joint (b, c). Opacification of the joint cavity on the dorsal and palmar side confirmed adequate CA administration (arrowhead). Please note the absence of communication between the radiocarpal and middle carpal joint. (c) The needle was safely intra-articular if the bevel of the needle was in the respective centre from the joint space. (d) radiographic control for extraarticular contrast leakage and CA distribution in the second plane. Please note the carpometacarpal joint cavity irregular appearance and the always distal extending and attaching to the proximal metacarpal bones at varying heights (arrowheads); the palmar recess of the middle carpal joint extended to the carpometacarpal joint I (arrow).

frequency of 15–18 MHz. Each carpus was examined before and after each injection of CA. The following data were collected: start/attachment of joint capsule, number of recesses, localization of recesses, shape of recesses, extension of recesses, anatomic relationship, distribution pattern of CA, echogenicity and pattern/structure.

2.5 | Evaluation

All radiographic, computed tomographic, ultrasonographic and 3D-VRT images and recorded data were evaluated and compared. The results and anatomical structures were compared with the literature (Entani et al., 2022; González-Rellán et al., 2021; González-Rellán et al., 2022; Hermanson, 2013; Mikić et al., 1992). Image viewing and analysis were performed and generated using medical imaging software Horos™ (version 3.3.6, <http://www.horos-project.org/>, open source, © 2022 Horos Project). Scan plane, window level and width and the zoom within the individual imaging study could be modified.

3 | RESULTS

The results of this study provide a morphological description of the arthrographic findings on US, CT, and radiography of artificially injected canine carpal joints and comprise the images presented in Figures 3–16. All 14 dogs showed for all modalities the same basic pattern in all carpi without side differences and sufficient opacification with 0.5 mL injected CA in the antebrachiocarpal and middle carpal joint. The amount of synovial fluid presented in the joints before the CA injection was not visualized ultrasonographically, radiographically and computed tomographically. The aspirated volume of arthrocentesis from the antebrachiocarpal and middle carpal joint was ≤0.1 mL. Ultrasonographically, each carpal joint capsule had a heterogeneous echogenic appearance and were confluent with the articular bone surface (Figure 14b/2), the synovial-connective tissue interface was indistinct to identify and the joint capsule fused with the echoes of adjacent soft tissue (Figure 14b/3). All carpal recesses presented as generalized anechogenic to hypoechoic (Figure 14b/1) filled continuation of the

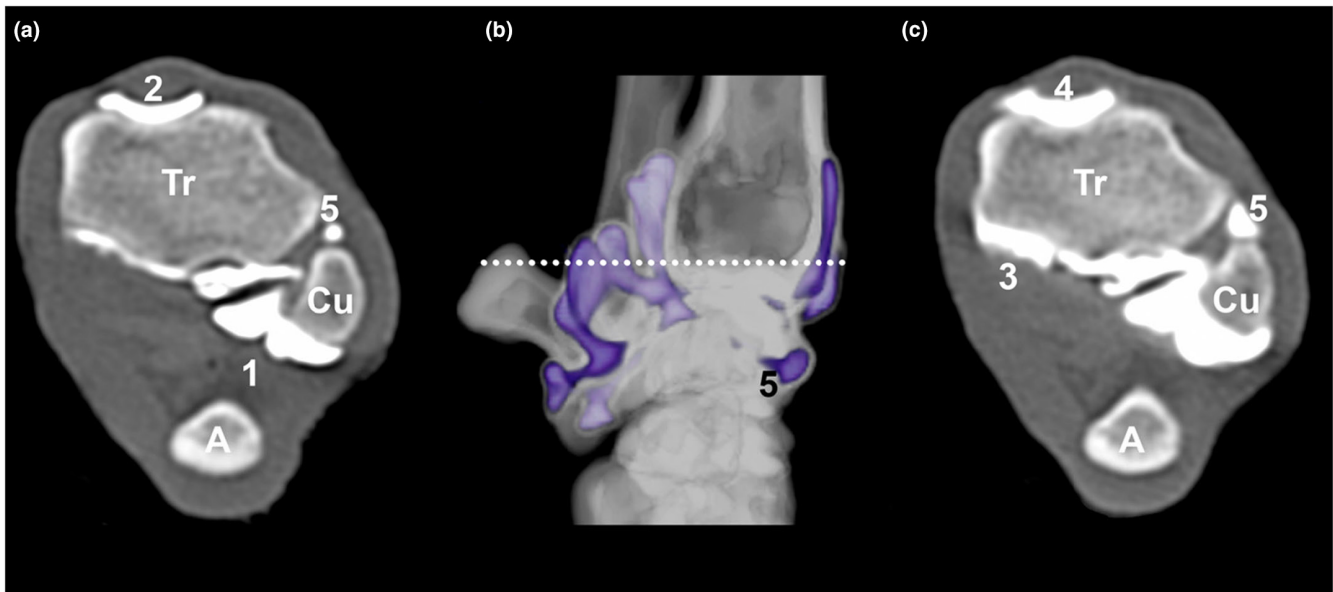


FIGURE 4 Distribution of CA of the antebrachicarpal joint with increasing CA volume. The middle image (b) shows a lateral VRT 3D image of a canine carpal arthrogram with 0.5 mL CA filling, the white dashed line indicates the level of the transverse CT arthrogram images with 0.5 mL (a) and 1.0 mL (c) CA filling. Window (WW = 500; WL = 2500). (A) accessory carpal bone; (Cu) head of ulna; (Tr) trochlea of radius. The CA filling of the antebrachicarpal joint first appeared mostly palmar with a palmarolateral (1) tendency as well as thin dorsoproximal (2) and dorsodistal (5), then thicker palmaromedial (3) and dorsoproximal (4), (5) distal radioulnar joint.

joint capsule with an indistinct peripheral hypoechoic to isoechoic fine capsule (Figure 14b/5). The basic pattern was as follows:

3.1 | Antebrachicarpal joint

The antebrachicarpal joint showed no synovial communication with the middle carpal joint, which always showed synovial communication with the carpometacarpal joint (Figure 3a,b). 0.5 mL CA filling of the antebrachicarpal joint appeared first palmar (Figure 4) with a palmarolateral tendency (Figure 4a/1) as well as thin dorsoproximal (Figure 4a/2) and dorsodistal (Figure 4b/5). Then with 1.0 mL CA filling palmaromedial (Figure 4c/3) and thicker dorsal (Figure 4c/4), 1.5 mL CA filling resulted in generalized joint filling.

The antebrachicarpal joint capsule released dorsal two map-like recesses. The dorsoproximal recess (Figure 5a-c/2) started broad-based at the craniodistal edge of the radius, filled completely the groove of extensor carpi radialis (Figure 5a/1) below the extensor carpi radialis longus et brevis muscle (Figure 5a/3) and ended at the level of the epiphyseal line (Figure 5c/1). The groove of extensor carpi radialis, the extensor carpi radialis brevis muscle and the dorsal antebrachicarpal fat pad with its triangular shape proved to be a quickly found dorsal landmark (Figure 15 and 16). With increasing volume, the anechogenic joint filling between bone and fat pad can be traced (Figure 16b/3-4), which is compressed and displaced dorsally out of the bone bed (Figure 16b/2).

The dorsodistal recess (Figure 5a-c/4) started at the cranioproximal edge of the intermedioradial carpal bone and covered it mostly. The dorsoproximal and dorsodistal recess confluent to form the smaller drop shaped medial recess (Figure 5b/5) at the level of the

medial styloid process and the larger lateral recess (Figure 5b/6), which is squared and completely adjacent to the ulnar carpal bone. The palmar recesses showed a shape variance from teardrop-shaped (Figure 14b/1) to sac-like or irregular mushroom-like with a basic pattern of at least five recesses (Figure 9/3-7), one irregularly branched recess proximomedial to the radius (Figure 6/1), three further recesses proximolateral in the triangle of radius, ulna and accessory carpal bone (Figure 6/2-4), always one distolateral recess is located distal to the accessory carpal bone (Figure 6/5). There was CA filling of the distal radioulnar joint (Figure 4a,b/5).

3.2 | Middle carpal joint

The middle carpal joint was always associated with the carpometacarpal joint (Figure 3a,b). Tendency of CA distribution was not evident with certainty and the gradual volume increase led to more distension and generalized joint filling without a clear dominating shape. The dorsal middle carpal joint capsule began at the dorsodistal edge of the intermedioradial and ulnar carpal bone, continued circularly medially, laterally and palmarly, and ended at the dorso-proximal edge of the distal carpal bones (Figure 7a,b/arrow heads).

In the triangle of the intermedioradial carpal bone, the ulnar carpal bone and the carpal bone IV, there was a dorsal overlap of the dorsodistal antebrachicarpal recess and the middle carpal joint in neutral (Figure 8/1-2) and slightly flexed position (Figure 9/arrow head).

There were always two dorsal middle carpal joint recesses, one extended from the distal edge of the intermedioradial carpal bone and covered completely the proximal half of the carpal bone III

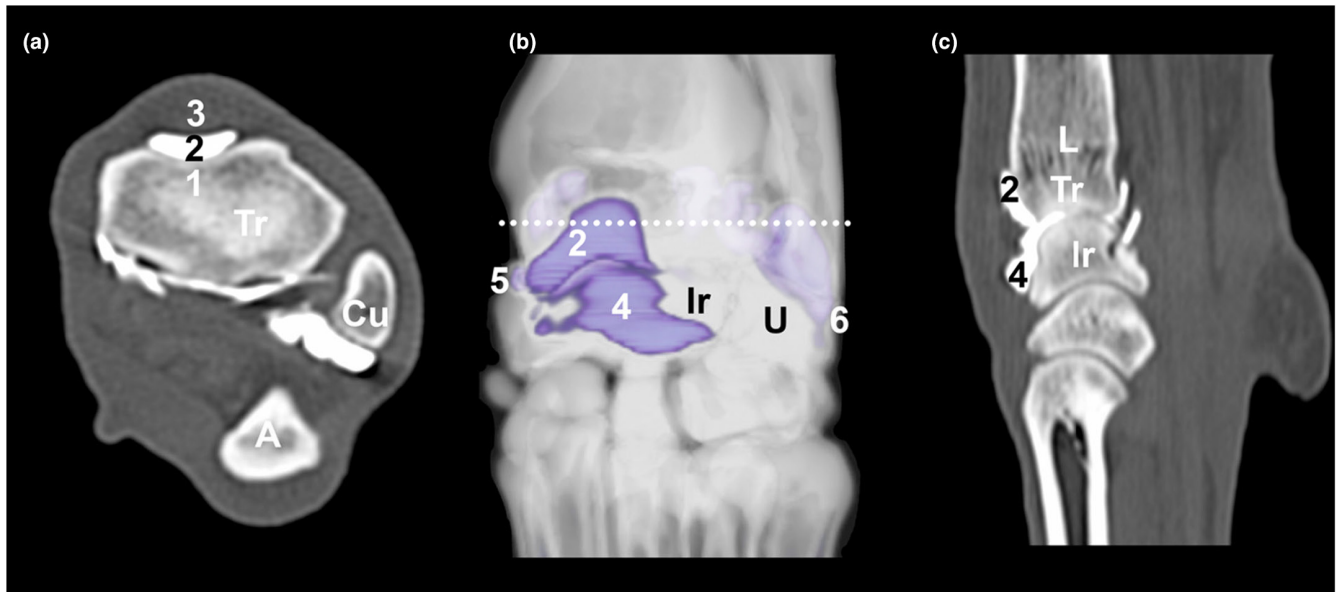


FIGURE 5 Dorsal, medial, and lateral antebrachiocarpal joint cavities and recesses. The middle image (b) shows a dorsal VRT 3D image of a canine carpal arthrogram with 0.5 mL CA filling of the antebrachiocarpal joint, the white dashed line indicates the level of the transverse (a) and sagittal (c) CT arthrogram images. Window (WW = 500; WL = 2500). (Tr) trochlea of radius; (Cu) head of ulna; (A) accessory carpal bone; (Ir) intermedioradial carpal bone (L) epiphysial line; (U) ulnar carpal bone. (1) groove of extensor carpi radialis; (2) dorsoproximal antebrachiocarpal recess; (3) extensor carpi radialis brevis muscle; (4) dorsodistal antebrachiocarpal recess; (5) medial antebrachiocarpal recess; (6) lateral antebrachiocarpal recess. Please note that in the dorsal VRT 3D image (b) the clear confluence to the lateral antebrachiocarpal recess was absent due to low CA volume.

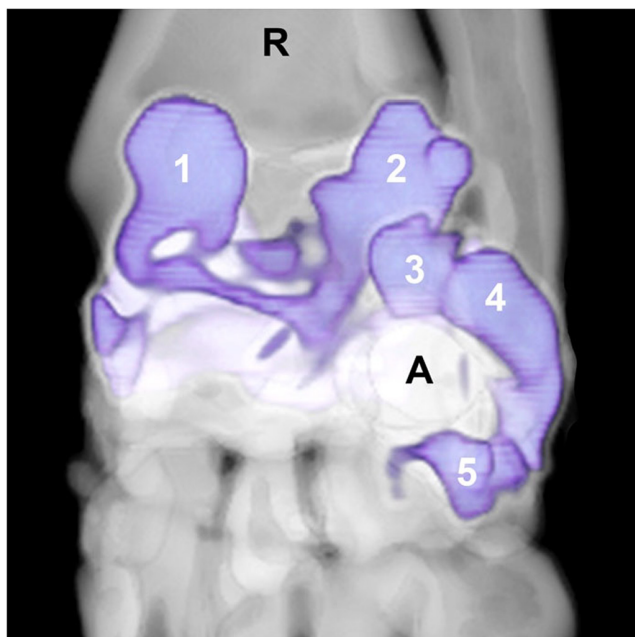


FIGURE 6 3D VRT CT image of the basic pattern of the five palmar antebrachiocarpal recesses. (A) accessory carpal bone; (R) radius; (1) proximomedial palmar antebrachiocarpal recess, (2–4) three proximolateral palmar antebrachiocarpal recesses, (5) distolateral palmar antebrachiocarpal recess.

(Figure 10a/1), the second extended from the distal edge of the ulnar carpal bone and covered the proximal two third of the carpal bone IV (Figure 10/2).

The middle carpal and the carpometacarpal joint formed a common drop-like medial (Figure 7a,b/4) and a lateral recess (Figure 7a,b/5). Proximally, the common medial recess was close to the distal end of the medial antebrachiocarpal recess, laterally it was not (Figure 10b/3-6).

In the palmar region there were always four recesses, the 1st almost completely covered the carpal bone I and extended to the carpometacarpal joint I without direct communication (Figure 3d/arrow), the 2nd one was between the intermedioradial carpal bone and the carpal bone III (Figure 11/8), the 3rd was between the ulnar carpal bone and the carpal bone IV (Figure 10a/7), the 4th recess (Figure 12/7), which was distal to the accessory carpal bone, extended from this.

3.3 | Carpometacarpal joint

The carpometacarpal joint filled in simultaneously with the injection of the middle joint.

Tendency of CA distribution was not evident with certainty and the gradual volume increase led to more distension and generalized joint filling. The carpometacarpal joint showed an irregular appearance without recognizing a constant pattern. The dorsal, medial, lateral and palmar joint capsule began close to the distal edge of the distal carpal bones, extended distally and attached to the proximal metacarpals at varying levels (Figure 3d/arrowheads). There were no clear dorsal and palmar recesses, they appeared here as funnel-shaped (Figure 12/8) and irregular, finely tubular extensions (Figure 11/10). Some conflated, extended dorsal and palmar along

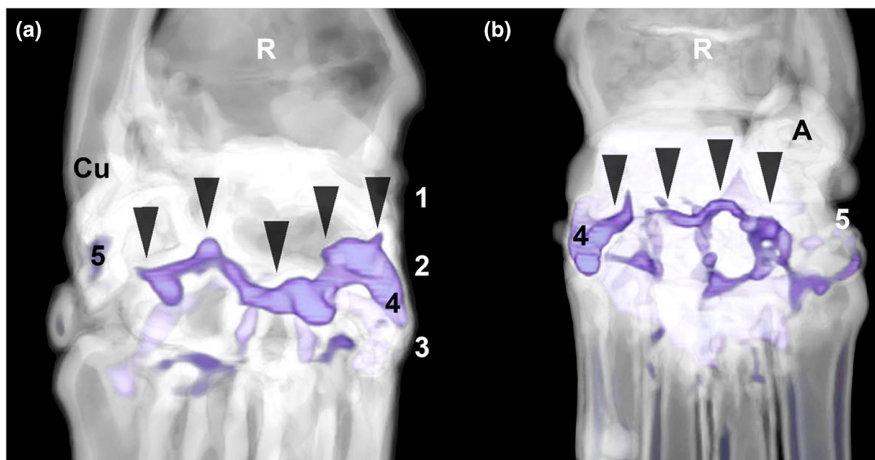


FIGURE 7 3D VRT CT images of the circularly running middle carpal joint cavity (arrow heads) in a dorsal (a) and palmar (b) view, isolated with 1.0 mL CA shown. (A) accessory carpal bone; (Cu) head of ulna; (R) radius; (1) antebrachiocarpal joint space; (2) middle carpal joint space; (3) carpometacarpal joint space; (4) common medial middle carpal and carpometacarpal recess; (5) common lateral middle carpal and carpometacarpal recess. The common lateral middle carpal and carpometacarpal recess was incompletely filled with contrast medium, the common fine confluence was visible.

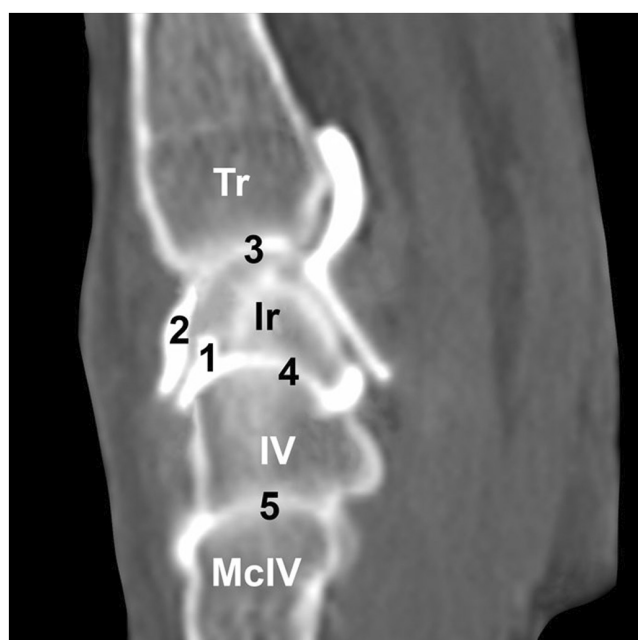


FIGURE 8 Sagittal CT arthrogram image of the overlap of the middle carpal joint with the part of the second dorsal middle carpal recess (1) with the dorsodistal antebrachiocarpal recess (2). Window (WW = 500; WL = 2500). (3) antebrachiocarpal joint space; (4) middle carpal joint space; (5) carpometacarpal joint space; (Ir) intermedioradial carpal bone; (McIV) metacarpal IV; (Tr) trochlea of radius; (IV) carpal bone IV.

the metacarpals I–V as well as in the intermetacarpal space. The most distal extension reached the level of the proximal metacarpal diaphysis (Figure 13). The most prominent finely tubular extension (Figure 11/9) runned dorsal to metacarpal III. Only ultrasonographically, the dorsal and palmar carpometacarpal tubular extensions could not be visualized distally.

3.4 | Extravasation

CA outside the joints along the needle tract occurred, but did not interfere with the evaluation of the images. In all dogs, 1.5 mL CA within in the antebrachiocarpal and the middle carpal joint generated back pressure with return flow into the syringe, and in seven dogs a small drop-shaped leak of CA occurred at the middle carpal joint when the needle was pulled out. Four carpi with extravasation more than needle tract or one drop CA leakage were not part of the study. Two carpi with a soft tissue defect due to improper storage and four carpi with degenerative changes were not included in this study.

4 | DISCUSSION

The aim of the present study was to provide a description of the morphological appearance of the canine carpal joint cavities and recesses using US, radiography, helical CT and 3D-VRT arthrography images. The novel results of this study provide the first morphological description of the ultrasonographic, radiographic and computed tomographic arthrographic appearance of the canine carpal joint cavities and recesses with different injection volumes. The canine carpal joint cavities and in particular its recesses had a complex appearance with a basic structure found in all dogs. The previous general description from the available literature (Evans & de Lahunta, 2013; Frewein et al., 2004; Horowitz & Berg, 2010; König et al., 2007; Mikić et al., 1992) are comprehensible, but in comparison to the results of this study, they only describe a part of the complex appearance. The described wide dorsal pouch of the antebrachiocarpal joint and the dorsal pouch of the middle carpal joint (Frewein et al., 2004) are comprehensible, at the antebrachiocarpal joint it presented as two recesses, the dorsoproximal antebrachiocarpal and the dorsodistal antebrachiocarpal recess, and at

FIGURE 9 Slightly flexed radiographic (a) and fluoroscopic (b) images of the arthrogram, contrast was injected with a 27 G needle (n) in the dorsal middle carpal joint under fluoroscopic control. There was an overlap (arrowhead) of the dorsal middle carpal joint (1) with the dorsodistal antebrachio-carpal recess (2). Please note the 5 clear basic palmar antebrachio-carpal recesses (3–7).

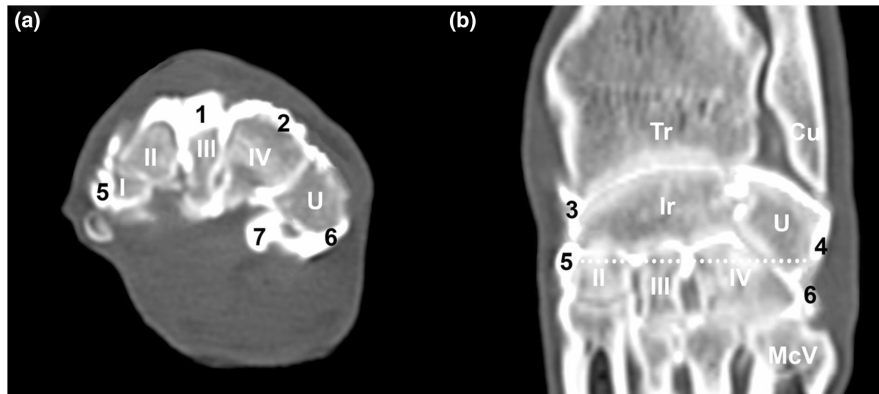
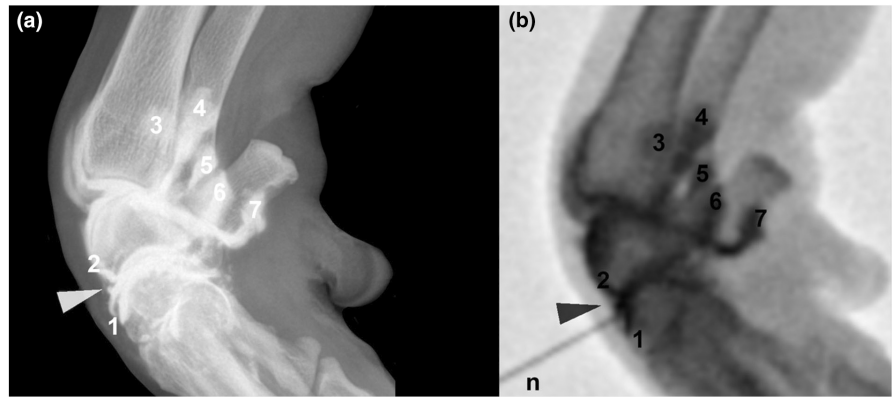


FIGURE 10 Transverse (a) and sagittal (b) CT arthrogram images of the 2 dorsal middle carpal recesses. Window (WW=500; WL=2500). The white dashed line indicates the level of the transverse CT arthrogram image. (Cu) head of ulna; (I) carpal bone I; (II) carpal bone II; (III) carpal bone III; (IV) carpal bone IV; (Ir) intermediocarpal bone; (McV) metacarpal V. (Tr) trochlea of radius; (U) ulnar carpal bone; (1) first dorsal middle carpal recess; (2) second dorsal middle carpal recess; (3) medial antebrachio-carpal recess; (4) lateral antebrachio-carpal recess; (5) common medial middle and carpometacarpal recess; (6) common lateral middle and carpometacarpal recess; (7) third palmar middle carpal recess.

the middle carpal joint it represented as two dorsal middle carpal recesses. The generally described multiple recesses of the antebrachio-carpal joint (Mikić et al., 1992) are in agreement with our results, their anatomical location, shape, and number were described precisely in this study.

Regardless of the size difference, the already described dorsal overlap of the antebrachio-carpal and the middle carpal joint in the cat (Basa et al., 2022) was also presented in all dogs. In our study, the antebrachio-carpal joint was always punctured first, there was no incorrect joint puncture of the middle carpal joint due to the dorsal overlap of the antebrachio-carpal joint and the middle carpal joint. In the clinical setting, diseased joints may differ morphologically from healthy joints; therefore, the dorsal overlap should be considered in diseased joints. For example, only the antebrachio-carpal joint may be altered or filled and mistakenly punctured as the middle carpal joint or vice versa, especially if the carpus is insufficiently flexed during puncture.

In veterinary medicine, arthrocentesis (Torres & Duerr, 2020) or arthrography (Reis Silva et al., 2013) can be performed 'blindly' with anatomical landmarks. In this study, correct needle placement was performed using anatomical landmarks (Vollmerhaus, 2007) and confirmed by fluoroscopy. Three types of extravasation occurred.

In addition to the subtle extravasation along the needle tract, which is interpreted for technical reasons, a small drop-shaped leak occurred when the needle was withdrawn in seven dogs with an injection volume of 1.5 mL CA in the middle carpal joint. The cause is not interpreted to be a malpuncture of the joint, but rather the pressure created due to the high injection volume. Diffuse dorsal extravasation and long-range contrast distribution in the extensor tendon sheath occurred in four study-excluded cadavers and can be considered as an arthrographic puncture failure. Post-mortem changes such as adhesions or a physiological connection would be other causes of direct communication between the tendon sheath and the joint cavity. For safe puncture of the joint cavity, in addition to using anatomical landmarks, it is recommended to lateralise and fixate the tendon structures with the fingers and to check the final position of the needle using US, fluoroscopy or radiography.

A further aim of this study was to prove the applicability of musculoskeletal US for the detection of carpal joint effusion in dogs using three ascending artificial joint fillings. For this purpose, all examined dogs were clinically and radiologically normal and had no joint effusion. The physiological carpal synovial volume is described as a drop of up to 1 mL (Clements, 2006; Cowell & Valenciano, 2014; Whitelock, 2001) in the literature. In our study, the aspirated volume

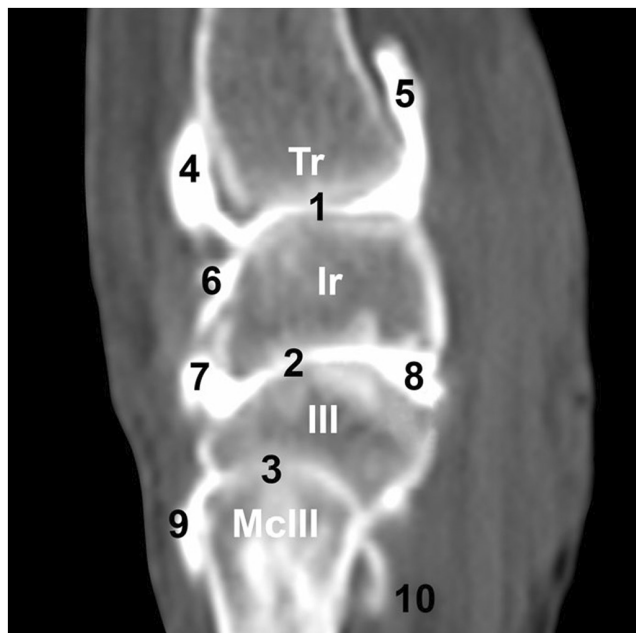


FIGURE 11 Overview of the dorsal and palmar carpal recesses, sagittal CT arthrogram image. Window (WW = 500; WL = 2500). (III) carpal bone III; (Ir) intermedioradial carpal bone; (McIII) metacarpal III; (Tr) trochlea of radius; (1) antebrachioarpal joint space; (2) middle carpal joint space; (3) carpometacarpal joint space; (4) dorsoproximal antebrachioarpal recess; (5) proximolateral palmar antebrachioarpal recess; (6) dorsodistal antebrachioarpal recess; (7) first dorsal middle carpal recess; (8) second palmar middle carpal recess; (9) tubular dorsal carpometacarpal extension; (10) finely tubular palmar carpometacarpal extension.

of arthrocentesis from the antebrachioarpal and middle carpal joint was ≤ 0.1 mL, thus, all carpi were in the lower range of the described reference value and had no joint effusion. This amount of synovial fluid presented in the joints before the CA injection was not visualized ultrasonographically, radiographically and computed tomographically. All artificial joint fillings could be visualized, demonstrating the applicability of US in the detection of artificial carpal effusion. This result should be transferable to clinical patients with carpal effusion. However, not all results from cadavers can necessarily be transferred to clinical patients, it must be considered that the synovial volume was either physiologically low or was reduced by the freezing process, it is also unclear whether the freezing process altered the fine joint capsule and recesses. Healthy carpal joints without a freezing process or an animal experiment are required for a reliable evaluation to draw conclusions about physiological canine carpal joint filling or joint effusion. Our injected volumes can be used as a guide for further research in canine carpal effusion.

A different pattern of contrast distribution from the antebrachioarpal joint is described in the cat compared to the dog, the feline antebrachioarpal joint tends to occur dorsally and distally first, with the palmar joint cavity filling last with CA (Basa et al., 2022). CA filling of the canine antebrachioarpal joint always appeared initially palmarolaterally pronounced and dorsally thin without dorso-proximal or dorsodistal tendency, then palmaromedially and thicker



FIGURE 12 Overview of the palmar carpal recesses, 3D VRT CT arthrogram image in palmar view with 1.0 mL CA filling in both antebrachioarpal and middle carpal joint. For a better understanding, please compare with the isolated filled antebrachioarpal joint from Figure 2. (A) accessory carpal bone; (1) proximomedial palmar antebrachioarpal recess; (2–4) proximolateral palmar antebrachioarpal recesses; (5) lateral antebrachioarpal recess; (6) distolateral palmar antebrachioarpal recess; (7) fourth palmar middle carpal recess; (8) palmar carpometacarpal funnel-like extension; (9) first palmar middle carpal recess; (10) medial common middle carpal and carpometacarpal recess; (11) medial antebrachioarpal recess.

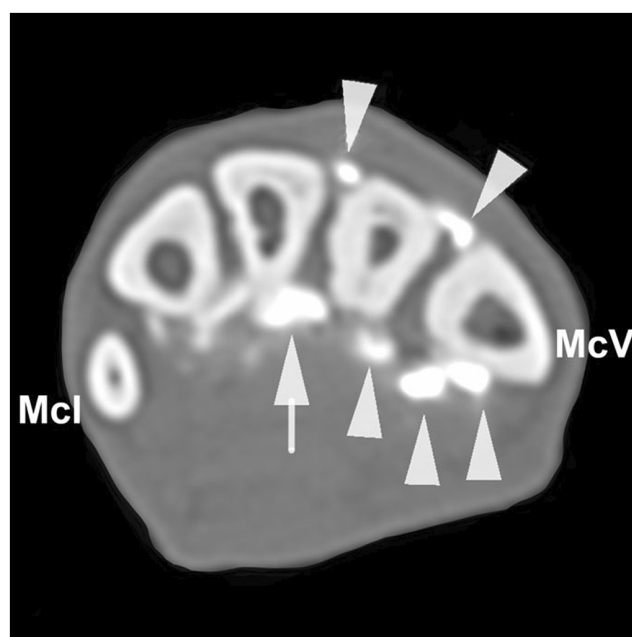


FIGURE 13 Transverse CT arthrogram image of the dorsal intermetacarpal and palmar carpometacarpal extensions, tubular (arrowheads) and confluent (arrow), at the level of the proximal metacarpal diaphysis. (Mcl) metacarpal I; (McV) metacarpal V.

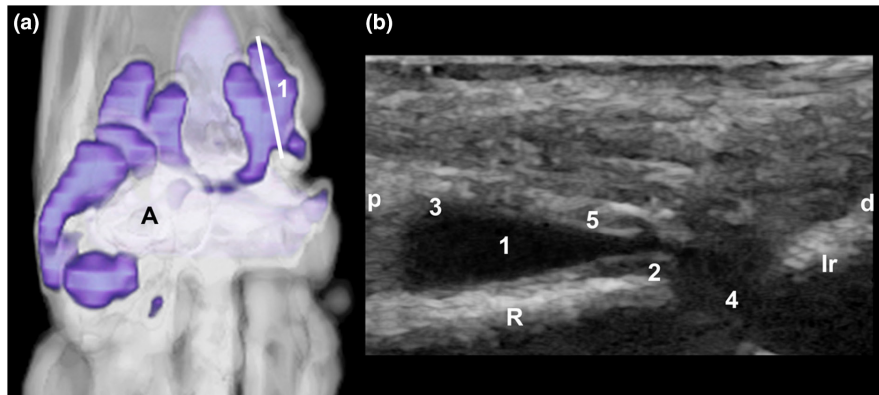


FIGURE 14 Sagittal ultrasonographic image (b) of the teardrop-shaped proximalateral palmar antebrachioarpal recess, the white oblique line in the 3D VRT CT arthrogram image in palmar view (a) shows the corresponding transducer position. (A) accessory carpal bone; (Ir) intermedioradial carpal bone; (R) radius; (p) proximal; (d) distal; (1) anechoic proximalateral palmar antebrachioarpal recess; (2) joint capsule; (3) synovial-connective tissue interface; (4) antebrachioarpal joint space; (5) indistinct peripheral hypoechoic to isoechoic fine recess capsule.

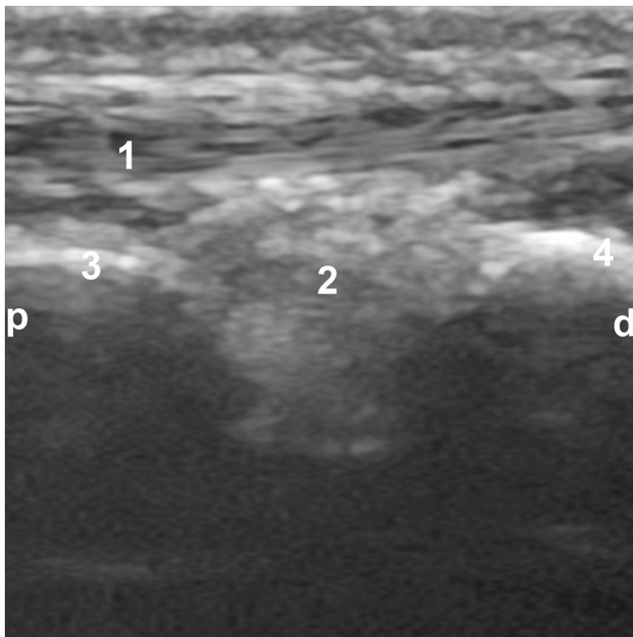


FIGURE 15 Sagittal ultrasonographic image of the unfilled dorsal antebrachioarpal recess. (p) proximal; (d) distal; (1) extensor carpi radialis brevis muscle; (2) dorsal antebrachioarpal fat pad; (3) groove of extensor carpi radialis; (4) intermedioradial carpal bone.

dosally. Disregarding the fact that an artificial joint effusion may not have the same distribution as a naturally occurring joint effusion, the canine distribution pattern suggested that a low-grade antebrachioarpal joint effusion is clinically and radiographically difficult to detect or undetectable. Despite the variance of the recesses and the multitude of variable US positions for detection, an US examination with palmarolateral and dorsal focus is recommended, especially in questionable clinical situation or joint effusion. The sagittal plane is preferred, which allowed a better overview, and may enable imaging of two or three joint spaces together on one sonogram.

US and CT arthrography with the colour image creation of the 3D-VRT were reliable methods to identify the artificially injected joint fillings. All recesses could be visualized ultrasonographically. Carpometacarpal were no clear dorsal and palmar recesses, they appeared here as tubular extensions along the metacarpals I–V, which could not be visualized distally by US. The maximum distal end represented the proximal metacarpal diaphysis. The most prominent finely tubular extension runned dorsal to metacarpal III. In case of injury or an open metacarpal fracture, the anatomical position of the carpometacarpal joint with the finely tubular extension on metacarpus III should be taken into account with regard to joint involvement. Especially as metacarpal fractures are common in dogs (Muir & Norris, 1997), and most fractures affected the body followed by the base of metacarpus III (Kornmayer et al., 2014).

The limitations of the present study were, first, the heterogeneity and the number of included dogs, which did not permit analyses transferable to the whole canine population. Additional studies are necessary to generate this data in specific breeds and sizes to characterize what a veterinarian will observe in a clinical setting. Second, the results were obtained by a combination of three imaging techniques alone compared with the current literature, histological studies would be conceivable. Third, the US examination was performed with one US probe, a wide-band interoperative linear array transducer. Further examinations with different US probes and lower US frequencies would be useful, as a high-frequency transducer is not always available in the clinical setting and different equipment is used. Fourth, the technically necessary pressure to be applied for optimal coupling was not standardized and may led to variable results.

In conclusion, this study provided a complete description of the appearance of the canine carpal joint cavities and their recesses. In clinically absent or unclear carpal joint effusion, US assists the practitioner in deciding to perform an arthrocentesis by visualizing the joint effusion. Further studies about ultrasonographic characteristics of carpal disorders and the sensitivity and applicability are required.

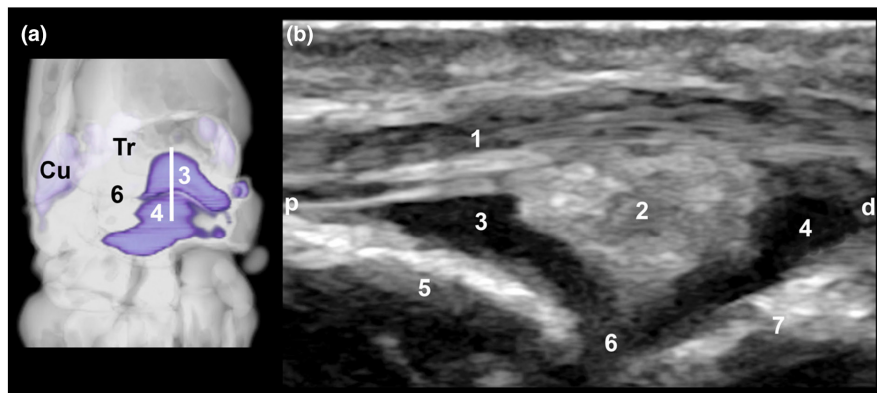


FIGURE 16 Sagittal ultrasonographic image (b) of the filled dorsal antebrachiocarpal recess, the white line in the 3D VRT CT arthrogram image in dorsal view (a) shows the corresponding transducer position. (Cu) head of ulna; (Tr) trochlea of radius; (p) proximal; (d) distal; (1) extensor carpi radialis brevis muscle; (2) dorsal antebrachiocarpal fat pad; (3) dorsoproximal antebrachiocarpal recess; (4) dorsodistal antebrachiocarpal recess; (5) groove of extensor carpi radialis; (6) dorsal antebrachiocarpal joint space; (7) intermedioradial carpal bone. Please compare with [Figure 13](#) and note the dorsal displacement of the antebrachiocarpal fat pad.

ACKNOWLEDGEMENTS

We are deeply indebted to the many colleagues and friends who offered intellectual guidance and valuable advice. Open Access funding enabled and organized by Projekt DEAL.

CONFLICT OF INTEREST STATEMENT

The authors declare that there is no conflict of interest.

DATA AVAILABILITY STATEMENT

The data that support the findings of this study are available from the corresponding author S.K. Whenever possible, the persistent identifier (DOI) was inserted along the reference.

ORCID

Sven Klußmann  <https://orcid.org/0009-0000-1491-045X>

Andrea Meyer-Lindenberg  <https://orcid.org/0000-0001-6137-3773>

Andreas Brühnschwein  <https://orcid.org/0000-0002-7833-8031>

REFERENCES

- Adams, J. E., Zobitz, M. E., Reach, J. S., Jr., An, K. N., Lewallen, D. G., & Steinmann, S. P. (2005). Canine carpal joint fusion: A model for four-corner arthrodesis using a porous tantalum implant. *The Journal of Hand Surgery*, 30(6), 1128–1135. <https://doi.org/10.1016/j.jhssa.2005.08.008>
- Allan, G., & Davies, S. (2018). Radiographic signs of joint disease in dogs and cats. In D. E. Thrall (Ed.), *Textbook of veterinary diagnostic radiology* (Vol. 7, pp. 403–433). Elsevier. <https://doi.org/10.1016/B978-0-323-48247-9.00033-4>
- Alsafy, M. A. M., El-Gendy, S. A. A., & Abou-Ahmed, H. M. (2015). The carpal joint of the donkey (*Equus asinus*): Morphological investigation. *International Journal of Morphology*, 33, 948–954. http://www.scielo.cl/scielo.php?script=sci_arttext&pid=S0717-9502201500300023&nrm=iso
- Basa, R. M., Crowley, A. M., & Johnson, K. A. (2020). Neurofibroma of the ulnar nerve in the carpal canal in a dog: Treatment by marginal neurectomy. *The Journal of Small Animal Practice*, 61(8), 512–515. <https://doi.org/10.1111/jsap.12945>
- Basa, R. M., Johnson, K. A., & Podadera, J. M. (2022). The effect of CT and MRI with and without arthrography on the appearance of the feline carpal ligaments. *BMC Veterinary Research*, 18(1), 368. <https://doi.org/10.1186/s12917-022-03463-6>
- Beccati, F., Gialletti, R., Passamonti, F., Nannarone, S., Di Meo, A., & Pepe, M. (2015). Ultrasonographic findings in 38 horses with septic arthritis/tenosynovitis. *Veterinary Radiology & Ultrasound*, 56(1), 68–76. <https://doi.org/10.1111/vru.12183>
- Bristow, P. C., Meeson, R. L., Thorne, R. M., Butterworth, S. J., Rutherford, S., Renwick, A. I. C., Wustefeld-Janssens, B., Witte, P. G. K., Woods, S., Parsons, K. J., Keeley, B. J., Owen, M. R., Li, A., & Arthurs, G. I. (2015). Clinical comparison of the hybrid dynamic compression plate and the castless plate for pancarpal arthrodesis in 219 dogs. *Veterinary Surgery*, 44, 70–77. <https://doi.org/10.1111/j.1532-950X.2014.12183.x>
- Castelli, E., Pozzi, A., Klisch, K., Scotti, L., Hoey, S., & Dennler, M. (2019). Comparison between high-field 3 tesla MRI and computed tomography with and without arthrography for visualization of canine carpal ligaments: A cadaveric study. *Veterinary Surgery*, 48(4), 546–555. <https://doi.org/10.1111/vsu.13186>
- Clements, D. (2006). Arthrocentesis and synovial fluid analysis in dogs and cats. *In Practice*, 28(5), 256–262. <https://doi.org/10.1136/inpract.28.5.256>
- Cowell, R. L., & Valenciano, A. C. (2014). *Cowell and Tyler's diagnostic cytology and hematology of the dog and cat*. Elsevier <https://books.google.de/books?id=bOTXIAEACAAJ>
- Denny, H. R., & Barr, A. R. S. (1991). Partial carpal and pancarpal arthrodesis in the dog: A review of 50 cases. *Journal of Small Animal Practice*, 32(7), 329–334. <https://doi.org/10.1111/j.1748-5827.1991.tb00943.x>
- De Rycke, L. M., Gielen, I. M., Dingemanse, W., Kromhout, K., & van Bree, H. (2015). Computed tomographic and low-field magnetic resonance arthrography: A comparison of techniques for observing intra-articular structures of the Normal canine shoulder. *Veterinary Surgery*, 44(6), 704–712. <https://doi.org/10.1111/vsu.12321>
- DeCamp, C. E., Johnston, S. A., Déjardin, L. M., & Schaefer, S. L. (2016). 14 - fractures and other orthopedic conditions of the carpus, metacarpus, and phalanges. In C. E. DeCamp, S. A. Johnston, L. M. Déjardin, & S. L. Schaefer (Eds.), *Brinker, Piermattei and Flo's handbook of small animal orthopedics and fracture repair* (Fifth ed., pp. 389–433). W.B. Saunders. <https://doi.org/10.1016/B978-1-4377-2364-9.00023-9>
- Eivers, C. R., Corzo-Menéndez, N., Austwick, S. H., Thomson, D. G., Gibson, S. M., Handel, I., & Schwarz, T. (2018). Computed

- tomographic arthrography is a useful adjunct to survey computed tomography and arthroscopic evaluation of the canine shoulder joint. *Veterinary Radiology & Ultrasound*, 59(5), 535–544. <https://doi.org/10.1111/vru.12670>
- El-Gendy, S. A. A., Alsafy, M. A. M., Rutland, C. S., El-Khamary, A. N., Abu-Ahmed, H. M., & El-Kammar, M. H. (2020). Morphological and imaging evaluation of the metacarpophalangeal and metatarsophalangeal joints in healthy and lame donkeys. *Journal of Equine Veterinary Science*, 88, 102904. <https://doi.org/10.1016/j.jevs.2019.102904>
- Entani, M. G., Franini, A., Barella, G., Saleri, R., De Rensis, F., & Spattini, G. (2022). High-resolution ultrasonographic anatomy of the carpal tendons of sporting border collies. *Animals*, 12(16), 2050 <https://www.mdpi.com/2076-2615/12/16/2050>
- Evans, H. E., & de Lahunta, A. (2013). Arthrology. In *Miller's anatomy of the dog* (Vol. 4th, pp. 158–184). Elsevier Health Sciences <https://books.google.de/books?id=6eBOAQAQBAJ>
- Farrow, C. S. (1982). Stress radiography: Applications in small animal practice. *Journal of the American Veterinary Medical Association*, 181(8), 777–784. <https://www.ncbi.nlm.nih.gov/pubmed/7141974>
- Ford, T. S., Ross, M. W., & Orsini, P. G. (1988). Communications and boundaries of the middle carpal and carpometacarpal joints in horses. *American Journal of Veterinary Research*, 49(12), 2161–2164.
- Frewein, J., Nickel, R., Schummer, A., & Seiferle, E. (2004). Knochen der Schultergliedmaße, Verbindungen der Knochen der Schultergliedmaße. In *Lehrbuch der Anatomie der Haustiere* (Vol. 8, pp. 67–97). Parey <https://books.google.de/books?id=VU4mNtNycG6YC>
- Gerdes, C., Morgan, R., Terry, R., Foote, A., & Smith, R. (2022). Computed tomographic arthrography, gross anatomy and histology demonstrate a communication between synovial invaginations in the proximal aspect of the third interosseous muscle and the carpometacarpal joint in horses. *Frontiers in Veterinary Science*, 9, 958598. <https://doi.org/10.3389/fvets.2022.958598>
- Getman, L. M., McKnight, A. L., & Richardson, D. W. (2007). Comparison of magnetic resonance contrast arthrography and arthroscopic anatomy of the equine palmar lateral outpouching of the middle carpal joint. *Veterinary Radiology & Ultrasound*, 48(6), 493–500. <https://doi.org/10.1111/j.1740-8261.2007.00286.x>
- González-Rellán, S., Barreiro, A., Cifuentes, J. M., & Fdz-de-Trocóniz, P. (2022). Anatomy of the palmar region of the carpus of the dog. *Animals (Basel)*, 12(12), 1573. <https://doi.org/10.3390/ani12121573>
- González-Rellán, S., Fdz-de-Trocóniz, P., & Barreiro, A. (2021). Ultrasonographic anatomy of the dorsal region of the carpus of the dog. *Veterinary Radiology & Ultrasound*, 62(5), 591–601. <https://doi.org/10.1111/vru.13003>
- González-Rellán, S., Fdz-de-Trocóniz, P., & Barreiro, A. (2023). Ultrasonographic anatomy of the palmar region of the carpus of the dog. *Veterinary Radiology & Ultrasound*, 64(3), 546–556. <https://doi.org/10.1111/vru.13224>
- Gray, S. N., Puchalski, S. M., & Galuppo, L. D. (2013). Computed tomographic arthrography of the intercarpal ligaments of the equine carpus. *Veterinary Radiology & Ultrasound*, 54(3), 245–252. <https://doi.org/10.1111/vru.12033>
- Guilliard, M. J. (1997). Dorsal radiocarpal ligament sprain causing intermittent carpal lameness in high activity dogs. *The Journal of Small Animal Practice*, 38(10), 463–465. <https://doi.org/10.1111/j.1748-5827.1997.tb03442.x>
- Guilliard, M. J., & Mayo, A. K. (2000). Sprain of the short radial collateral ligament in a racing greyhound. *The Journal of Small Animal Practice*, 41(4), 169–171. <https://doi.org/10.1111/j.1748-5827.2000.tb03188.x>
- Haburjak, J. J., Lenehan, T. M., Davidson, C. D., Tarvin, G. B., Carlson, K. R., & Hayes, A. (2003). Treatment of carpometacarpal and middle carpal joint hyperextension injuries with partial carpal arthrodesis using a cross pin technique: 21 cases. *Veterinary and Comparative Orthopaedics and Traumatology*, 16, 105–111. <https://doi.org/10.1055/s-0038-1632760>
- Harris, A., & Santangelo, K. (2020). Joint fluid analysis and collection considerations. In F. M. Duerr (Ed.), *Canine Lameness* (pp. 111–123). John Wiley & Sons. <https://doi.org/10.1002/9781119473992.ch9>
- Hermanson, J. W. (2013). The muscular system. In H. E. Evans & A. de Lahunta (Eds.), *Miller's anatomy of the dog* (Vol. 4, pp. 185–280). Elsevier Health Sciences <https://books.google.de/books?id=6eBOAQAQBAJ>
- Hittmair, K. M., Groessl, V., & Mayrhofer, E. (2012). Radiographic and ultrasonographic diagnosis of stenosing tenosynovitis of the abductor pollicis longus muscle in dogs. *Veterinary Radiology & Ultrasound*, 53(2), 135–141. <https://doi.org/10.1111/j.1740-8261.2011.01886.x>
- Horowitz, A., & Berg, R. (2010). Thoracic limb. In K. D. Budras (Ed.), *Anatomy of the dog* (Vol. 5, pp. 16–27). Schlütersche Verlagsgesellschaft mbH & Company KG <https://books.google.de/books?id=kEuBQAQBAJ>
- Jerram, R. M., Walker, A. M., Worth, A. J., & Kuipers von Lande, R. G. (2009). Prospective evaluation of pancarpal arthrodesis for carpal injuries in working dogs in New Zealand, using dorsal hybrid plating. *New Zealand Veterinary Journal*, 57(6), 331–337. <https://doi.org/10.1080/00480169.2009.60927>
- Johnson, K. A. (1987). Accessory carpal bone fractures in the racing greyhound Classification and Pathology. *Veterinary Surgery*, 16(1), 60–64. <https://doi.org/10.1111/j.1532-950x.1987.tb00914.x>
- König, H. E., Liebich, H. G., & Bragulla, H. (2007). Vorder-oder Schultergliedmaßen. In *Anatomie der Haussäugetiere: Lehrbuch und Farbatlas für Studium und Praxis* (Vol. 3, pp. 141–210). Wiley <https://books.google.de/books?id=QoXiBjSp368C>
- Kornmayer, M., Failing, K., & Matis, U. (2014). Long-term prognosis of metacarpal and metatarsal fractures in dogs. A retrospective analysis of medical histories in 100 re-evaluated patients. *Veterinary and Comparative Orthopaedics and Traumatology*, 27(1), 45–53. <https://doi.org/10.3415/vcot-13-03-0038>
- Li, A., Bennett, D., Gibbs, C., Carmichael, S., Gibson, N., Owen, M., Butterworth, S. J., & Denny, H. R. (2000). Radial carpal bone fractures in 15 dogs. *The Journal of Small Animal Practice*, 41(2), 74–79. <https://doi.org/10.1111/j.1748-5827.2000.tb03167.x>
- Marcellin-Little, D. J., & von Pfeil, D. J. F. (2020). Carpal Region. In F. M. Duerr (Ed.), *Canine Lameness* (pp. 169–193). John Wiley & Sons. <https://doi.org/10.1002/9781119473992.ch13>
- McQuillan, S., Kearney, C., Hoey, S., Connolly, S., & Rowan, C. (2022). A threshold volume of 10 ml is suggested for detecting articular cartilage defects in equine carpal joints using CT arthrography: Ex vivo pilot study. *Veterinary Radiology & Ultrasound*, 63(1), 54–63. <https://doi.org/10.1111/vru.13028>
- Mikić, Ž. D., Ercegan, G., & Somer, T. (1992). Detailed anatomy of the antebrachiocarpal joint in dogs. *The Anatomical Record*, 233(2), 329–334. <https://doi.org/10.1002/ar.1092330217>
- Milgram, J., Stockman, J., Segev, G., Meiner, Y., & Shipov, A. (2019). Contribution of palmar radiocarpal and ulnocarpal ligaments to the stability of the canine Antebrachiocarpal joint. *Veterinary and Comparative Orthopaedics and Traumatology*, 32(4), 305–313. <https://doi.org/10.1055/s-0039-1685208>
- Moser, T., Dosch, J.-C., Moussaoui, A., & Dietemann, J.-L. (2007). Wrist ligament tears: Evaluation of MRI and combined MDCT and MR arthrography. *American Journal of Roentgenology*, 188(5), 1278–1286. <https://doi.org/10.2214/ajr.06.0288>
- Muir, P., & Norris, J. L. (1997). Metacarpal and metatarsal fractures in dogs. *The Journal of Small Animal Practice*, 38(8), 344–348. <https://doi.org/10.1111/j.1748-5827.1997.tb03482.x>
- Neville-Towle, J. D., Tan, C. J., Parr, W. C. H., Walsh, W. R., & Johnson, K. A. (2018). Three-dimensional kinematics of the canine carpal bones imaged with computed tomography after ex vivo axial limb

- loading and palmar ligament transection. *Veterinary Surgery*, 47(6), 861–871. <https://doi.org/10.1111/vsu.12921>
- Nordberg, C. C., & Johnson, K. A. (1999). Magnetic resonance imaging of normal canine carpal ligaments. *Veterinary Radiology & Ultrasound*, 40(2), 128–136. <https://doi.org/10.1111/j.1740-8261.1999.tb01897.x>
- Parker, R. B., Brown, S. G., & Wind, A. P. (1981). Pancarpal arthrodesis in the dog: A review of forty-five cases. *Veterinary Surgery*, 10(1), 35–43. <https://doi.org/10.1111/j.1532-950X.1981.tb00627.x>
- Pownder, S. L., Cooley, S., Hayashi, K., Bezuidenhout, A., Koff, M. F., & Potter, H. G. (2016). Non-invasive magnetic resonance imaging diagnosis of presumed intermedioradial carpal bone avascular necrosis in the dog. *The Canadian Veterinary Journal*, 57(8), 879–881. <https://www.ncbi.nlm.nih.gov/pubmed/27493290>
- Reis Silva, H., Uosyete, R., Clements, D. N., Bergkvist, G. T., & Schwarz, T. (2013). Computed tomography and positive contrast computed tomographic arthrography of the canine shoulder: Normal anatomy and effects of limb position on visibility of soft tissue structures. *Veterinary Radiology & Ultrasound*, 54(5), 470–477. <https://doi.org/10.1111/vru.12054>
- Reising, A. J., Donnelly, L. L., Flesner, B. K., Maitz, C. A., & Bryan, J. N. (2021). Solitary osseous plasmacytomas in dogs: 13 cases (2004–2019). *The Journal of Small Animal Practice*, 62(12), 1114–1121. <https://doi.org/10.1111/jsap.13411>
- Rondeau, M. P., Walton, R. M., Bissett, S., Drobatz, K. J., & Washabau, R. J. (2005). Suppurative, nonseptic Polyarthropathy in dogs. *Journal of Veterinary Internal Medicine*, 19(5), 654–662. <https://doi.org/10.1111/j.1939-1676.2005.tb02743.x>
- Salomon, F. V. (2020). Bewegungsapparat. In F. V. Salomon, H. Geyer, & U. Gille (Eds.), *Anatomie für die Tiermedizin* (Vol. 4, pp. 36–248). Thieme. [10.1055/b-007-168897](https://doi.org/10.1055/b-007-168897)
- Samii, V. F., Dyce, J., Pozzi, A., Drost, W. T., Mattoon, J. S., Green, E. M., Kowaleski, M. P., & Lehman, A. M. (2009). Computed tomographic arthrography of the stifle for detection of cranial and caudal cruciate ligament and meniscal tears in dogs. *Veterinary Radiology & Ultrasound*, 50(2), 144–150. <https://doi.org/10.1111/j.1740-8261.2009.01507.x>
- Shaughnessy, M. L., Sample, S. J., Abicht, C., Heaton, C., & Muir, P. (2016). Clinical features and pathological joint changes in dogs with erosive immune-mediated polyarthritis: 13 cases (2004–2012). *Journal of the American Veterinary Medical Association*, 249(10), 1156–1164. <https://doi.org/10.2460/javma.249.10.1156>
- Suarez Sanchez-Andrade, J., Richter, H., Kuhn, K., Bischofberger, A. S., Kircher, P. R., & Hoey, S. (2018). Comparison between magnetic resonance imaging, computed tomography, and arthrography to identify artificially induced cartilage defects of the equine carpal joints. *Veterinary Radiology & Ultrasound*, 59(3), 312–325. <https://doi.org/10.1111/vru.12598>
- Théoret, M. C., & Moens, N. M. (2007). The use of veterinary cuttable plates for carpal and tarsal arthrodesis in small dogs and cats. *The Canadian Veterinary Journal*, 48(2), 165–168. <https://www.ncbi.nlm.nih.gov/pmc/articles/PMC1780233/pdf/cvj48pg165.pdf>
- Tnibar, M., Kaser-Hotz, B., & Auer, J. A. (1993). Ultrasonography of the dorsal and lateral aspects of the equine carpus: Technique and normal appearance. *Veterinary Radiology & Ultrasound*, 34(6), 413–425. <https://doi.org/10.1111/j.1740-8261.1993.tb02030.x>
- Tobolska, A., Adamiak, Z., & Głodek, J. (2020). Clinical applications of imaging modalities of the carpal joint in dogs with particular reference to the Carpal Canal. *J Vet Res*, 64(1), 169–174. <https://doi.org/10.2478/jvetres-2020-0006>
- Torres, B. T., & Duerr, F. M. (2020). Arthrocentesis technique. In F. M. Duerr (Ed.), *Canine Lameness* (pp. 93–104). John Wiley & Sons. <https://doi.org/10.1002/9781119473992.ch7>
- Vaughan, L. C. (1985). Disorders of the carpus in the dog II. *British Veterinary Journal*, 141(5), 435–446. <https://doi.org/10.1016/0007-1935>
- Vollmerhaus, B. (2007). Gelenkpunktion (Arthrozentese). In H. Schebitz & W. Brass (Eds.), *Operationen an Hund und Katze* (pp. 19–24). Parey <https://books.google.de/books?id=MPD306OmNLOC>
- Warnock, J. J., & Beale, B. S. (2004). Arthroscopy of the antebrachio-carpal joint in dogs. *Journal of the American Veterinary Medical Association*, 224(6), 867–874. <https://doi.org/10.2460/javma.2004.224.867>
- Whitelock, R. (2001). Conditions of the carpus in the dog. *In Practice*, 23(1), 2–13. <https://doi.org/10.1136/inpract.23.1.2>
- Willer, R. L., Johnson, K. A., Turner, T. M., & Piermattei, D. L. (1990). Partial carpal arthrodesis for third degree carpal sprains. A review of 45 carpi. *Veterinary Surgery*, 19(5), 334–340. <https://doi.org/10.1111/j.1532-950x.1990.tb01201.x>
- Yalden, D. W. (1970). The functional morphology of the carpal bones in carnivores. *Acta Anatomica (Basel)*, 77(4), 481–500. <https://doi.org/10.1159/000143557>

How to cite this article: Klußmann, S., Meyer-Lindenberg, A., & Brühshwein, A. (2024). Arthrographic description of the canine carpal joint cavities and its recesses. *Anatomia, Histologia, Embryologia*, 53, e13026. <https://doi.org/10.1111/ahe.13026>